Mechanical Properties of 3Y-TZP Woodpile Scaffold Made by Extrusion 3D Printing

Patrick de Lima Gomes[a,b] 🔟 *, Victor Ribeiro de Miranda[c], Isabela Santana de Oliveira[a],*

Juliana Kelmy Macário Barboza Daguano[d]* 🔟 *, Carlos Nelson Elias[b]* 🔟 *, Claudinei dos Santos[a,c]* 🔟

[a]*Universidade Federal Fluminense, Escola de Engenharia Metalúrgica Industrial de Volta Redonda, Volta Redonda, RJ, Brasil.*
[b]*Instituto Militar de Engenharia, Seção de Engenharia de Materiais, Rio de Janeiro, RJ, Brasil.*
[c]*Universidade do Estado do Rio de Janeiro, Faculdade de Tecnologia, Resende, RJ, Brasil.*
[d]*Centro de Tecnologia da Informação Renato Archer, Grupo de Biofabricação, Campinas, SP, Brasil.*

Zirconia woodpile scaffolds (3Y-TZP/PL, n = 20), designed with null inter-filament spacing, were manufactured using the Direct Ink Writing (DIW), an extrusion 3D printing technique. A ceramic ink containing 40%v/v 3Y-TZP powder, 59%v/v PEG (Polyethylene glycol)/Laponite ink, and 1%v/v DBP (Dibutylphthalate) was used. For 3D printing, we used Ø 0.63 mm nozzles, a printing speed of 10 mm/s, a cross-layer deposition strategy, and no air gaps between filaments. The scaffolds were sintered at 1550 °C for 2 h. The mechanical characterization involved measurements of X-ray diffraction, scanning electron microscopy, Vickers microhardness, Vickers nanohardness, and modulus of elasticity and compressive strength. The sintered samples showed predominantly the ZrO_2-tetragonal phase and a microstructure characterized by a bimodal distribution of grain sizes. The samples had a relative density of 90.1 ±1.5%, a Vickers microhardness of 1172 ±45 HV, a Vickers nanohardness of 1608 ±78 HV, a modulus of elasticity of 203 ±16 GPa, and a compressive strength of 192 ±54 MPa. The results showed that DIW processing followed by proper sintering is a promising method for making zirconia scaffolds for biomedical applications.

Keywords: *Additive manufacturing, DIW, 3Y-TZP, bioceramics, mechanical properties.*

1. Introduction

Yttria-stabilized zirconia (Y-TZP) is a ceramic used as a biomaterial, especially in the manufacturing of dental prostheses. Y-TZP has a hardness of about 1250 HV, an elastic modulus of about 200 GPa, a flexural strength of about 800 MPa, and a fracture toughness of about 7 MPa·m$^{1/2}$. Y-TZP has toughening mechanisms due to the stress-induced phase transformation from tetragonal to monoclinic, which reduces crack propagation[1]. Among the different zirconia compositions, 3Y-TZP (ZrO_2 - 3 mol.% Y_2O_3) has the highest mechanical strength due to a higher percentage of the tetragonal phase. The 5Y-PSZ zirconia (ZrO_2 - 5 mol.% Y_2O_3) offers better optical properties due to a more significant proportion of the cubic phase but lower mechanical strength. These characteristics make Y-TZP ceramics a viable option for dental prostheses and implant components[2,3].

Additive Manufacturing (AM) is a technique based on material deposition in successive layers[4], which enables the rapid production of parts. AM processes begin with the creation of a 3D model using CAD software. The 3D model is converted into a .stl file and sliced into individual layers by software. The data is then transferred to the AM equipment, which builds the 3D objects by adding successive layers[5,6]. Although AM initially involved only polymeric and metallic materials, advances in methodologies and equipment have made it possible to manufacture ceramic materials.

Research has shown that AM ceramics, when sufficiently densified within their limits, have properties that can meet the mechanical requirements for various applications, such as high compressive strength, making them suitable for special applications such as single-unit dentures, where the masticatory loading stresses are mostly compressive[7-9]. The possibility of developing products with antibacterial properties in dentistry has also been explored[10-13].

Direct Ink Writing (DIW) is a material extrusion process useful for advanced applications involving complex geometries impractical with other manufacturing processes. High-quality DIW ink formulations require refined powders, suspensions with high solid content, and polymeric additives. Moreover, the processing and sintering parameters are crucial for improving the properties of the final product. It is noteworthy that the deposition of layers in an orthogonal orientation (woodpile) constitutes one of the most stable and prevalent forms of printing in this technique, commonly referred to as a scaffold structure[14,15].

Studies have focused on the impact of pore size and porosity on the mechanical properties of scaffolds. The present study aims to manufacture and characterize ceramic samples based on 3Y-TZP. The specimens were produced using the DIW technique. The samples were subsequently sintered in an effort to achieve a solid structure with no air gaps between filaments. The effects of null inter-filament spacing on the mechanical properties of

woodpile scaffolds were investigated. The evaluation of the samples included analysis of printing parameters and sintering conditions. The objective of this analysis was to obtain three-dimensional ceramic structures that exhibit mechanical properties suitable for applications in dental prostheses.

2. Experimental Procedure

2.1. Processing

This study used the ceramic powder of 3Y-TZP zirconia (G2DY-020OO, SINOCERA, China). Table 1 summarizes

Table 1. Summary of the characteristics of the raw powders used in this study, as provided by the manufacturers.

Powder characteristics (wt.%)	Laponite XLG (BYK)	3Y-TZP (SINOCERA, G2DY-020OO)
Y_2O_3	-	3.40 - 3.70
SiO_2	59.5	-
Na_2O	2.8	-
Li_2O	0.8	-
MgO	27.5	-
ZrO_2	-	balance
Specific surface area (m^2/g)	370	9.00 -11.5
Density (g/cm^3)	2.53	6.05
Melting temperature (°C)	900	2715

the main characteristics of this powder, including chemical composition, density, particle size, and specific surface area. To improve the extrudability and structural stability of the ink, 7.5% v/v of Laponite XLG (BYK/Colormix Ltda., Brazil) a nanosilicate powder, rheological modifier, and gel former, was added to an aqueous solution of 44.4% v/v of Polyethylene Glycol (PEG) 400 (380-420 g.mol^{-1}, Dinamica Ltda., Brazil) in deionized water. Dibutyl phthalate (DBP with 278.35 g.mol^{-1}, Synth, Brazil) was also used at 1% v/v as a rheological modifier in the ink. The remaining volume (40% v/v) was filled by incorporating ZrO_2 ceramic powder.

Figure 1 shows the development of the PEG-Laponite ink and a flowchart of the preparation and 3D printing of the samples, including sintering and characterization of the final product. The gel base, containing the same additives (PEG-Laponite-DBP) previously mentioned, had its rheology investigated in earlier studies[16,17]. The present work replaced only the zirconia source used in the ink preparation.

2.2. 3D printing by extrusion

The fabrication of ceramic prototypes was carried out using a DIW-type 3D printer equipped with a two syringes extrusion head (3D iCan X dual, ICAN, Brazil). The 10 mL disposable syringes with Luer lock connections (Descarpack, Brazil) were fitted with conical nozzles of 630 μm diameter (20G, Nordson EFD, USA). The printing process occurred at room temperature (25 ±2 °C), with a relative humidity of 60-65%. The prismatic structures (10.7 x 10.7 x 17.6 mm) were built layer by layer, totaling 32 layers with 18 filaments per layer and no air gaps between the filaments. The deposition strategy involved perpendicular cross-layer stacking. More
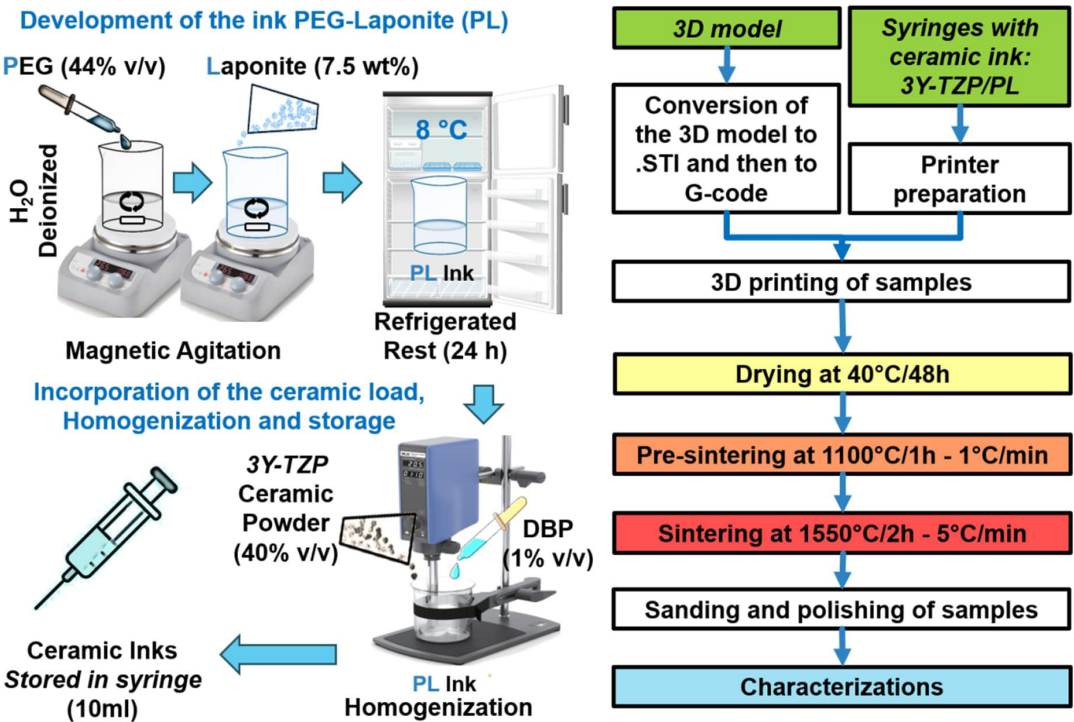

Figure 1. Flowchart for the development of 3Y-TZP/PL ceramic ink and subsequent steps.

details on the geometry and printing strategy can be found in Figure 2.

After printing, the samples were heated in an oven at 40 °C for 48 hours. Once dried, the green-printed structures had enough strength for manual handling and were transferred from the printing platform to the furnace. They underwent pre-sintering at 1100 °C for 1 h, with heating and cooling rates of 1 °C/min and 5 °C/min, respectively. This step aimed to remove the binders and organic additives, minimizing sample deformation and cracking risk. Subsequently, the samples were sintered according to the following thermal cycle:

- heating from room temperature to 600 °C at a rate of 10 °C/min;
- additional heating to 1550 °C at a rate of 5 °C/min, maintaining this temperature for 2 h;
- cooling from 1550 °C to room temperature at a rate of 5 °C/min.

2.3. Characterizations

Using the Archimedes method in distilled water at room temperature, the apparent density was measured following ASTM B962 (2017)[18]. The correlation between the measured apparent density and the real density of the samples was used to estimate the relative density. The real density of the sintered 3Y-TZP-laponite ceramics was determined by helium-pycnometry using an Ultrapyc 1200e, V5.04 pycnometer. Sintered samples were fragmented, sieved (<25μm), compacted (Ø20mm x 3mm height), and then measured in duplicate for ten cycles per specimen.

The sintered samples and as-received powders were analyzed using X-ray diffraction (XRD). The experiment used a Panalytical (Empyrean model, Malvern PANalytical, UK) with Cu-Kα radiation. Data was analyzed using X'pert-Highscore (Phillips) software and the ICDD database. The experiment was conducted over a 2θ range of 10° to 90°, with a step size of 0.01°/s and a scan rate of 100 s.

Scanning Electron Microscopy (SEM) (Mira 3 XMU model, Tescan, Czech Republic) was used to analyze the surface microstructure. The samples were prepared by grinding and polishing with a 1 μm diamond solution. The samples were then heat-treated at 1400 °C for 15 min and sputter-coated with Au. Surface images were acquired at 20 kV, and the microstructural features were treated using *Image-J* software.

The Vickers microhardness (HV) was measured on ceramic samples using a Durometer (HMV-G model, Shimadzu, Japan) with a Vickers micro-indenter. The procedure involved applying a 9.8 N load for 30 s and conducting 20 indentations on the sample (ASTM C1327-15)[19]. The nanohardness was investigated through nanoindentation of the polished surface of the samples. An ultra microdurometer (DUH – 211S model, Shimadzu, Japan) was used, with loads of 1000 mN and a maximum penetration depth of 10 μm. Young's modulus was calculated based on the Oliver and Pharr model[20,21]. The values represent the average of 10 nanoindentations for each selected load, with the error expressed as a standard deviation.

Compression testing was conducted on 20 samples using a universal testing machine (DL10000, EMIC, Brazil) with a 20 kN load cell and a 1 mm/min rate. The top and bottom surfaces were ground and polished with diamond paste to 6 μm while maintaining the parallelism of the surfaces. The dimensions after sintering were 8.1 x 8.1 x 13.4 mm, with a slight height reduction of about 0.3 mm. The area for compressive stress calculation was 65.6 mm[2]. The results were analyzed using Weibull statistics, a tool to model the probability distribution of failure and estimate stress values with high reliability for ceramic scaffolds.

3. Results and Discussion

3.1. Characterization of sintered samples

After sintering, the average relative density of the 3D-printed samples was 90.1 ± 1.5%. These results reflect the porosity profile of scaffolds built with cross-layer filament deposition. Figure 3 shows details of the filament layers in the green-printed samples. In these simulations, it is possible to observe that extensive macroscopic void formation occurs even with no gap between filaments. The voids were not eliminated during sintering, resulting in a residual porosity of
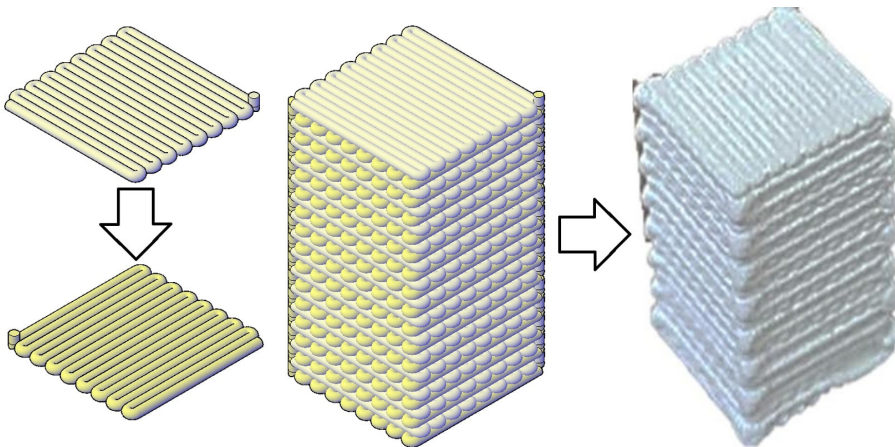

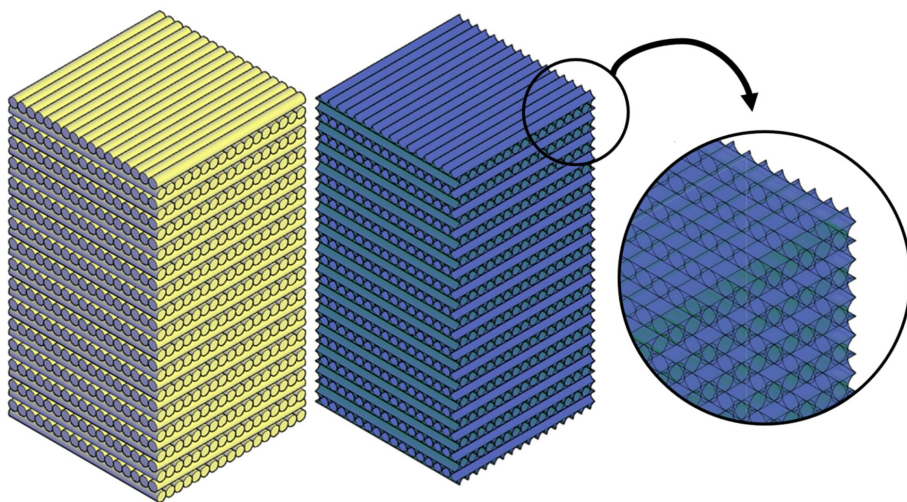**Figure 2.** Realistic layout of the layers and printed parts with 3Y-TZP/PL woodpile scaffolds.

Figure 3. (Yellow) layout of the printed ceramic ink layers; (Blue) simulation of the distribution of interconnected voids among the layers.

7.9%. The voids have a homogeneous distribution throughout the layers and among filaments.

Figure 4 shows the XRD results. The 3Y-TZP/PL samples are characterized by three main polymorph phases: 7% m-ZrO_2, 66% t- ZrO_2, and 27% c+t'- ZrO_2. Notably, the cubic (c) and pseudocubic (t') phases exhibit similar behavior and peak intensities.

Figure 5 shows the SEM images of the samples. The samples showed a bimodal grain size distribution. The scaffold had a grain size higher than expected for zirconia grains. The grains are surrounded by a matrix of ZrO_2 grains smaller than 1 μm. The 3Y-TZP/PL larger grains had more than 5 μm. During the sintering process, the constituents of the Laponite nanosilicate fuse during heating, resulting in an intergranular glassy phase composed of Si, Mg, Na, Li, and O. This phase did not change the zirconia stability during the pre-sintering process at 1100 °C because these elements remain in an amorphous state. With the heating at temperatures above 1450 °C, the viscosity of the glass resulting from the Laponite fusion decreases, intensifying chemical interactions between the intergranular vitreous phase components and the zirconia matrix. When the samples were heated to 1550 °C, some components of this residual liquid phase contributed to the destabilization or migration of Y_2O_3 present in the ZrO_2 grains. This can be attributed to increased diffusivity in these grains, which facilitates migration to the preferential grains, transforming small tetragonal grains into larger cubic phase grains. This phenomenon has also been discussed in the infiltration of 3Y-TZP ceramics with silicate glasses[22], supporting this hypothesis.

3.2. Mechanical properties of sintered samples

Figure 6 shows the microhardness, nanohardness, elastic modulus, and compressive strength results.

The 3Y-TZP/PL scaffold had a Vickers microhardness of 1172 ±45 HV and a Vickers nanohardness of 1608 ±78 HV. Both values are slightly lower than those reported in the literature[23-25].

As expected, printed ceramic scaffolds have higher nanometric hardness than micrometric hardness because pores
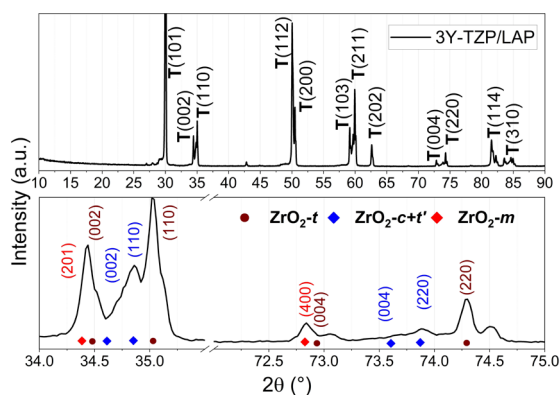

Figure 4. XRD pattern of the printed sample sintered at 1550°C for 2 h.

have a reduced influence on the nanoscale. Therefore, it is recommended to perform measurements in regions with low porosity, away from pores, edges, and other indentations, to avoid measurement errors. This procedure is more difficult to achieve in microhardness tests, where the indentation size typically encompasses several micropores, reducing the recorded hardness.

Another property calculated through Vickers nanoindentation was the elastic modulus, which averaged 203.52 ±16.34 GPa. This value is close to that found in the literature for dense ZrO_2[26]. Once again, due to the number and size of the pores in the prototype, no significant differences in elastic modulus were observed between the prototype with 92.1 ±3.4% relative density and pressed samples with higher relative densities.

The average compressive strength of the 3Y-TZP scaffolds ($n = 20$) was 191.5 ±53.7 MPa, with a Weibull modulus of 3.6 and a minimum compressive strength of about 120 MPa. The Weibull statistics and failure probability versus compressive stress graphs are presented in Figure 7. Due to their geometry, the scaffolds have a more fragile structure. The arrangement of the filaments and their circular shape lead to stress concentration
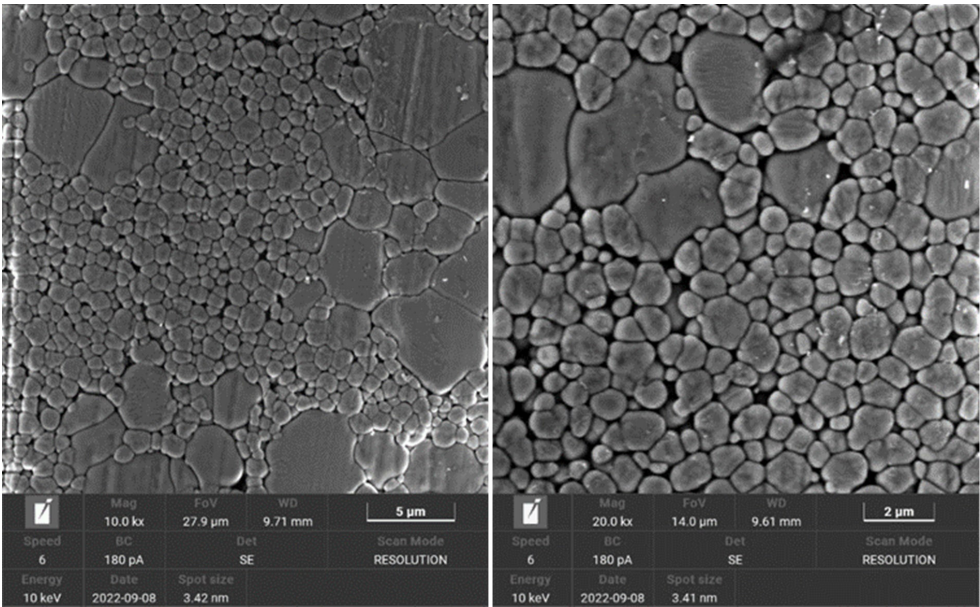
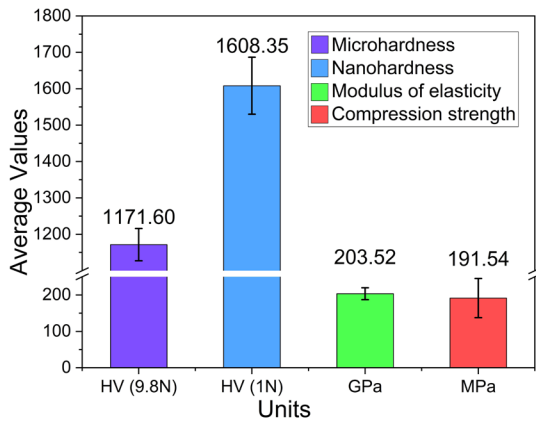**Figure 5.** SEM images of the sample sintered at 1550 °C for 2 h.

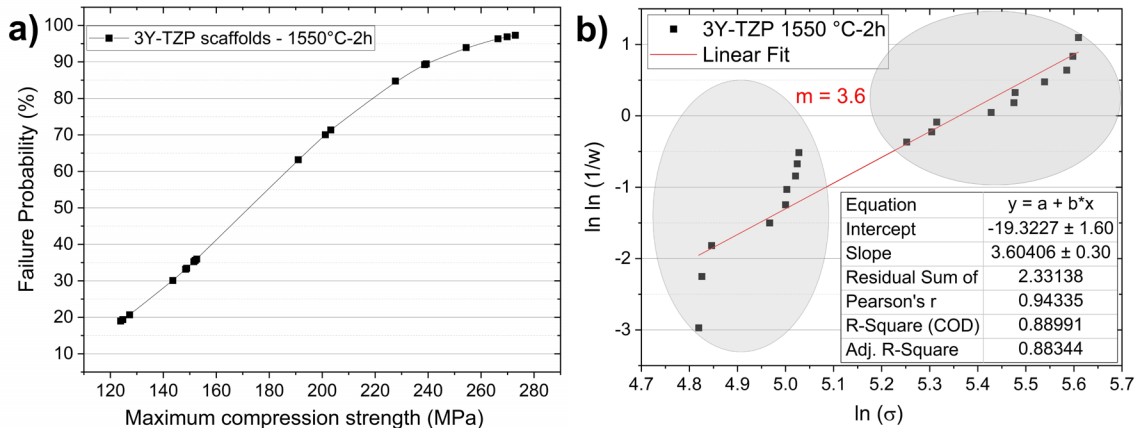**Figure 6.** Mechanical Properties of 3Y-TZP Scaffolds Sintered at 1550 °C for 2 h.

Figure 7. Weibull Modulus and Failure Probability of 3Y-TZP scaffold samples.

points and interconnected voids throughout the volume, resulting in lower strength compared to dense parts of similar dimensions. The Weibull statistics graph (Figure 7a) indicates a distribution of results into two groups with distinct mechanical behavior and well-defined stress values, as highlighted in the circles in Figure 7b. This suggests heterogeneities in the distribution of residual porosity and/or defects in different internal regions of the scaffolds. The defects induced fracture strength variation. It is recommended that future studies investigate the causes of this behavior. Nonetheless, one group of samples with superior mechanical performance showed significantly higher performance, with values ranging between 200 MPa and 280 MPa, while the other group exhibited compressive strength between 120 MPa and 160 MPa.

4. Conclusions

Based on the experimental data analysis, it concluded that
a) The ceramic ink prepared with a mixture of deionized water, PEG, DBP, and Laponite as additives has good extrudability and potential for AM of 3Y-TZP zirconia.
b) Using selected DIW parameters and a layer deposition strategy, 3Y-TZP woodpile scaffolds sintered at 1550 °C for 2 h achieved an average densification of more than 92%.
c) The interaction of Laponite components, mainly Mg, with yttria-stabilized tetragonal zirconia grains, leads to an increase in the growth of the ZrO_2-cubic phase. Combined with some residual porosity at the filament junctions, this contributes to the observed degradation of mechanical properties. The compressive strength displayed an average value of 191.54 ±53.76 MPa with a Weibull modulus of 3.6, which, although lower than for fully dense samples, remains within an adequate range for various applications and demonstrates high reliability below 120 MPa.

Within this study's experimental limits, the results indicate the possibility of producing high-solid-content ceramic inks for 3D printing using the DIW method, as well as the ability to fabricate 3D ceramic scaffolds with interesting mechanical properties and potential biomedical applications using 3Y-TZP-based ceramics. However, further improvements in compound formulations and 3D printing strategies are needed to optimize densification and improve mechanical properties such as compressive strength, thereby increasing the reliability of the final product.

5. Acknowledgments

6. References

1. Wang H, Aboushelib MN, Feilzer AJ. Strength influencing variables on CAD/CAM zirconia frameworks. Dent Mater. 2008;24(5):633-8. http://doi.org/10.1016/j.dental.2007.06.030.

2. Aboushelib M, Kleverlaan C, Feilzer A. Microtensile bond strength of different components of core veneered all-ceramic restorations Part II: zirconia veneering ceramics. Dent Mater. 2006;22(9):857-63. http://doi.org/10.1016/j.dental.2005.11.014.

3. Kosmac T, Oblak C, Jevnikar P, Funduk N, Marion L. The effect of surface grinding and sandblasting on flexural strength and reliability of Y-TZP zirconia ceramic. Dent Mater. 1999;15(6):426-33. http://doi.org/10.1016/S0109-5641(99)00070-6.

4. ASTM: American Society for Testing and Materials. ISO/ASTM 52900:2021: additive manufacturing - general principles - fundamentals and vocabulary. 2nd ed. West Conshohocken: ASTM; 2021.

5. Cotteleer M, Holdowsky J, Mahto M. The 3D opportunity primer: the basics of additive manufacturing [Internet]. Westlake: Deloitte University Press; 2013 [cited 2024 Oct 28]. 18 p. Available from: https://www2.deloitte.com/content/dam/insights/us/articles/the-3d-opportunity-primer-the-basics-of-additive-manufacturing/DUP_718-Additive-Manufacturing-Overview_MASTER1.pdf

6. Gibson I, Rosen DW, Stucker B. Additive manufacturing technologies: rapid prototyping to direct digital manufacturing. Boston: Springer; 2010. Chapter 17, The use of multiple materials in additive manufacturing; 436-49. https://doi.org/10.1007/978-1-4419-1120-9_17.

7. Gibson I, Rosen D, Stucker B. Additive manufacturing technologies: 3D printing, rapid prototyping, and direct digital manufacturing. 2nd ed. New York: Springer; 2015. Chapter 17, Design for additive manufacturing; 399-435. https://doi.org/10.1007/978-1-4939-2113-3_17.

8. Deckers J, Vleugels J, Kruth JP. Additive manufacturing of ceramics: a review. J Ceram Sci Technol. 2014;5(4):245-60. http://doi.org/10.4416/JCST2014-00032.

9. Lakhdar Y, Tuck C, Binner J, Terry A, Goodridge R. Additive manufacturing of advanced ceramic materials. Prog Mater Sci. 2021;116:100736. http://doi.org/10.1016/j.pmatsci.2020.100736.

10. Saeed F, Muhammad N, Khan AS, Khan AS, Sharif F, Rahim A, et al. Prosthodontics dental materials: from conventional to unconventional. Mater Sci Eng C. 2020;106:110167. http://doi.org/10.1016/j.msec.2019.110167.

11. Daguano JKMB, Santos C, Alves MFRP, Silva JVL, Souza MT, Fernandes MHFV. State of the art in the use of bioceramics to elaborate 3D structures using robocasting. Int J Adv Med Biotechnol. 2019;2(1):55-70. http://doi.org/10.25061/2595-3931/IJAMB/2019.v2i1.28.

12. Li X, Qi M, Li C, Dong B, Wang J, Weir MD, et al. Novel nanoparticles of cerium-doped zeolitic imidazolate frameworks with dual benefits of antibacterial and anti-inflammatory functions against periodontitis. J Mater Chem B Mater Biol Med. 2019;7(44):6955-71. http://doi.org/10.1039/C9TB01743G.

13. Alharbi N, Wismeijer D, Osman RB. Additive manufacturing techniques in prosthodontics: where do we currently stand? A critical review. Int J Prosthodont. 2017;30(5):474-84. http://doi.org/10.11607/ijp.5079.

14. Feilden E, Blanca EG-T, Giuliani F, Saiz E, Vandeperre L. Robocasting of structural ceramic parts with hydrogel inks. J Eur Ceram Soc. 2016;36(10):2525-33. http://doi.org/10.1016/j.jeurceramsoc.2016.03.001.

15. M'Barki A, Bocquet L, Stevenson AW. Linking rheology and printability for dense and strong ceramics by direct ink writing. Sci Rep. 2017;7:6017. http://doi.org/10.1038/s41598-017-06115-0.

16. Gomes PL, Freitas BX, Azoubel RA, Alves MFRP, Daguano JKMB, Santos C. Direct ink writing of 3Y-TZP ceramics using PEG-Laponite® as additive. Ceram Int. 2023;49(16):26348-58. http://doi.org/10.1016/j.ceramint.2023.05.170.

17. Gomes PL, Freitas BX, Alves MFR, Olhero S, Santos KF, Dávila JL, et al. Development of zirconia-based ceramics stabilized

with different yttria contents shaped by extrusion 3D-printing. J Mater Res Technol. 2024;28:2909-23. http://doi.org/10.1016/j.jmrt.2023.12.168.

18. ASTM: American Society for Testing and Materials. ASTM B962-17: standard test methods for density of compacted or sintered Powder Metallurgy (PM) products using Archimedes' Principle. West Conshohocken: ASTM; 2017. http://doi.org/10.1520/B0962-17.

19. ASTM: American Society for Testing and Materials. ASTM C1327-15: standard test method for vickers indentation hardness of advanced ceramics. West Conshohocken: ASTM; 2019. http://doi.org/10.1520/C1327-15R19.

20. Oliver WC, Pharr GM. An improved technique for determining hardness and elastic modulus using load and displacement sensing indentation experiments. J Mater Res. 1992;7:1564-83. http://doi.org/10.1557/JMR.1992.1564.

21. Oliver WC, Pharr GM. Measurement of hardness and elastic modulus by instrumented indentation: advances in understanding and refinements to methodology. J Mater Res. 2004;19:3-20. http://doi.org/10.1557/jmr.2004.19.1.3.

22. Campos TMB, Marinho RMM, Ribeiro ADOP, Montanheiro TLA, Silva AC, Thim GP. Microstructure and mechanical properties of fully sintered zirconia glazed with an experimental glass. J Mech Behav Biomed Mater. 2021;113:104093. http://doi.org/10.1016/j.jmbbm.2020.104093.

23. Miyazaki T, Nakamura T, Matsumura H, Ban S, Kobayashi T. Current status of zirconia restoration. J Prosthodont Res. 2013;57(4):236-61. http://doi.org/10.1016/j.jpor.2013.09.001.

24. Piconi C, Maccauro G. Zirconia as a ceramic biomaterial. Biomaterials. 1999;20(1):1-25. http://doi.org/10.1016/S0142-9612(98)00010-6.

25. Čokić SM, Cóndor M, Vleugels J, Van Meerbeek B, Van Oosterwyck H, Inokoshi M, et al. Mechanical properties–translucency–microstructure relationships in commercial monolayer and multilayer monolithic zirconia ceramics. Dent Mater. 2022;38(5):797-810. http://doi.org/10.1016/j.dental.2022.04.011.

26. Monção AMS, Santos ED, Gomes PL, Amarante JEV, Freitas BX, Santos C. Effect of Y_2O_3 content on the mechanical and optical properties of zirconia-based dental ceramics. Ceramica 2023;69(392):278-87. http://doi.org/10.1590/0366-69132024703923512.